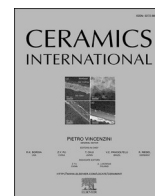




Contents lists available at ScienceDirect

Ceramics International

journal homepage: www.elsevier.com/locate/ceramint

Investigations for the effects of Ce-substitution on microstructure and magnetic properties of multi-doped YIG ferrites

Xiaoyi Wang^{a,b}, Kun Xu^a, Ning Ma^a, Xiujuan Feng^c, Gang Zhou^b, Gang Chen^a, Lei Zhao^{a,*}

^a School of Information and Control Engineering, China University of Mining and Technology, Xuzhou, 221116, Jiangsu Province, China

^b Yuyao Sunny Intelligent Optical Technology Co., Ltd, Ningbo, 315400, Zhejiang Province, China

^c School of Earth and Environment, Anhui University of Science and Technology, Huainan, 232001, Anhui Province, China

ARTICLE INFO

Handling Editor: Dr P. Vincenzini

Keywords:

Cerium substituted
YIG
Ferrite ceramics
Magnetic properties
Sintering temperature

ABSTRACT

In this paper, cerium (Ce) substituted YIG ferrite ceramics composed of $\text{Ca}_{0.3}\text{Ce}_x\text{Y}_{2.7-x}\text{Mn}_{0.05}\text{Zr}_{0.45}\text{Fe}_{4.5}\text{O}_{12}$ ($x = 0, 0.05, 0.1, 0.2, 0.3, 0.4, 0.5$) were synthesized by the conventional solid-state reaction route. The effects of Ce ions on properties of YIG products were investigated, it was found that the doping of Ce ions would not deteriorate crystal structure that all synthesized samples formed a YIG phase. On the other hand, the introduction of Ce ions had significant influences on morphologies, which would further affect magnetic properties. Besides, the influences of sintering temperature (1230 °C and 1280 °C) were also studied. The average grain size of the samples sintered at 1280 °C increased from 3.88 μm to 7.42 μm with the increase of Ce content, while the maximum average grain size was only 5.45 μm for the samples with a sintering temperature of 1230 °C. The value of saturated magnetization of the sample sintered at 1280 °C could reach up to 28.29 emu/g. In addition, the introduction of Ce ions could remarkably decrease the ferromagnetic resonance (FMR) linewidth for the samples sintered at 1280 °C. Specifically, the ΔH value of the prepared YIG sample is 867.3 Oe when no Ce dopant involved ($x = 0$). Then, the ΔH value sharply decreases to 541.6 Oe when the amount of Ce dopant is $x = 0.3$. Further increasing Ce concentration, the ΔH value can reach to 310 Oe when the amount of Ce dopant is $x = 0.5$. Therefore, the prepared Ce-doped YIG ferrite ceramics in this work have a promising application in microwave devices.

1. Introduction

As modern microwave communication technology progresses, microwave components are continuously evolving toward smaller sizes, lighter weights, and increased sensitivity [1–5]. Yttrium iron garnet (YIG) ferrite, is a kind of typical gyromagnetic ferrite characterized with its high saturation magnetization, high dielectric constant, low dielectric loss, and narrow ferromagnetic resonance (FMR) linewidth [6–11]. The narrow linewidth of ferromagnetic resonance of YIG has allowed important experimental studies on the microwave magnetic dynamics [12–14]. These exceptional electromagnetic properties make YIG gradually become an important part of magnetic spintronic devices and microwave communication devices, including circulators, phase shifters, and isolators [15–19]. Consequently, the development of YIG ferrite has garnered significant attention, presenting both significant challenges and vast opportunities for improving its various properties.

YIG possesses a cubic crystal structure with metal ions occupying

three different positions in a single cell of its *Ia3d* space group: Y^{3+} ions occupy the 24c dodecahedral position, and Fe^{3+} ions occupy the 16a octahedral and 24d tetrahedral positions. The super-exchange interactions between the magnetic metal cations give rise to magnetic moments in the YIG ferrites, especially between the Fe^{3+} ions locating at 16a and 24d positions [20–22]. There are also some studies that prove the existence of Fe^{2+} in YIG, which occupies tetrahedral or octahedral positions and thus affects the electromagnetic properties of YIG [23–25]. The generation and distribution of Fe^{2+} ions also have some influence on the electromagnetic properties of YIG. Leal et al. demonstrated that Y, Fe and Cu are mainly in the Y^{3+} , Fe^{3+} , Fe^{2+} and Cu^+ oxidation states in the Cu ion doped YIG, and that Cu^+ and Fe^{2+} cations prefer to occupy the octahedral sites in the YIG crystal structure [26]. Guerra et al. demonstrated that the Fe^{2+} cations and oxygen vacancies decrease as the Cr^{3+} cations concentration increases in the Er-Cr co-substituted YIG [27]. The addition of dopants can enhance magnetic properties YIG by replacing the positions of Y^{3+} and Fe^{3+} with doped ions [28–30]. In this regard,

* Corresponding author.

E-mail address: leizhao@cumt.edu.cn (L. Zhao).

<https://doi.org/10.1016/j.ceramint.2025.04.347>

Received 12 August 2024; Received in revised form 21 April 2025; Accepted 24 April 2025

Available online 24 April 2025

0272-8842/© 2025 Elsevier Ltd and Techna Group S.r.l. All rights are reserved, including those for text and data mining, AI training, and similar technologies.

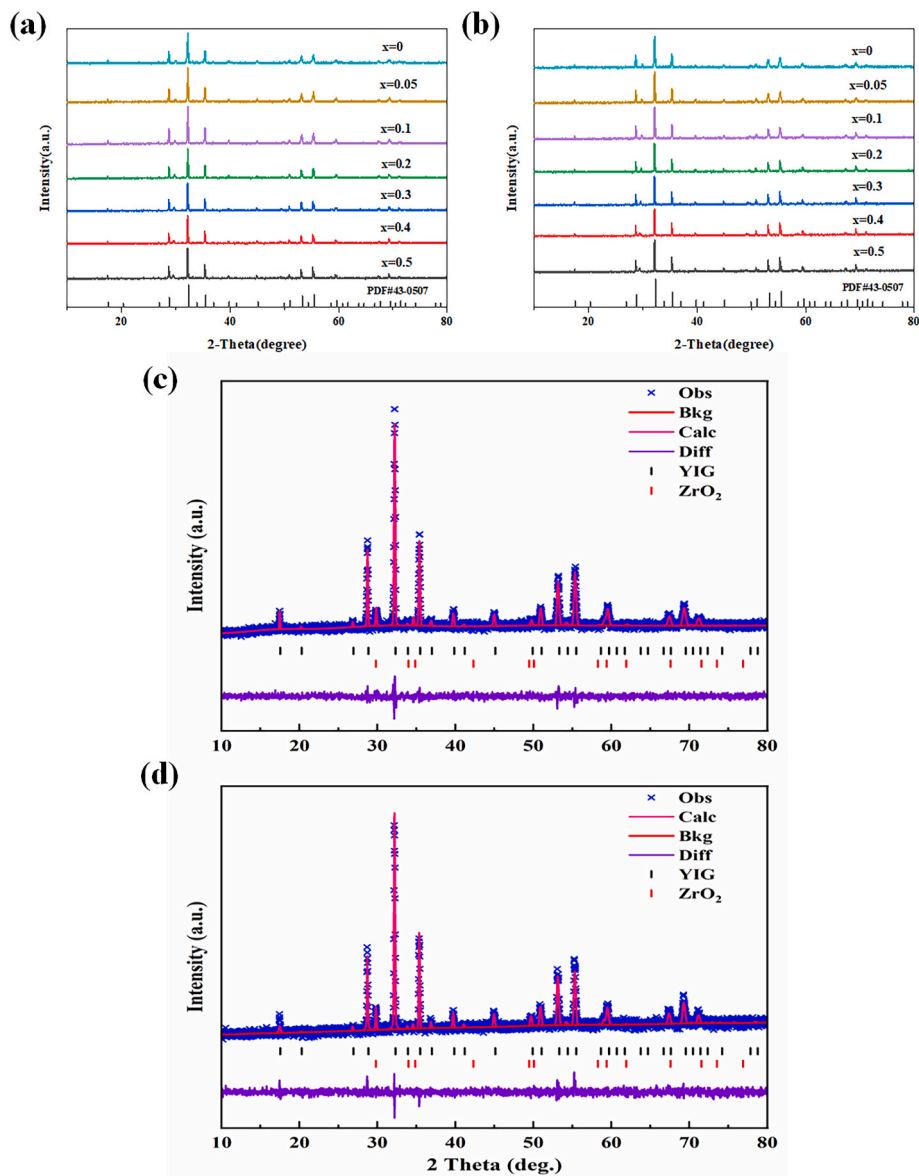


Fig. 1. (a) XRD patterns of the $\text{Ca}_{0.3}\text{Ce}_x\text{Y}_{2.7-x}\text{Mn}_{0.05}\text{Zr}_{0.45}\text{Fe}_{4.5}\text{O}_{12}$ samples (a) sintered at 1230 °C, (b) sintered at 1280 °C. Rietveld refinement of the XRD patterns of the samples (c) sintered at 1230 °C, (d) sintered at 1280 °C.

many scholars have carried out studies on the effects of different transition metal and rare earth elements doping and co-doping on microstructure and electromagnetic properties of YIG ferrites.

For example, Peña-García et al. revealed that that Zn^{2+} ions substitute the Fe^{2+} in octahedral positions. The total magnetic moment increases at low doping concentrations and decreases at high doping concentrations [31]. Caland et al. confirmed the preferential site occupancy of Ni in the yttrium iron garnet and that Y, Ni and Fe are predominantly in the Y^{3+} , Ni^{2+} , Fe^{3+} and Fe^{2+} oxidation states [32]. Li et al. revealed that the substitution of In ions would not change the crystal structure of YIG phase, while the existence of In ions could increase the bulk density. As the content of In ions increased up to $x = 0.45$, not only the saturation magnetization (M_s) increased to a maximum value, but also the narrowest ferromagnetic resonance line width (ΔH) was obtained [33]. Wang et al. revealed that Ca-Zr co-substituted YIG ferrites could hold a higher saturation magnetization and improve the electromagnetic properties [34]. Gao et al. synthesized Ca-Ge co-substituted YIG ferrites, which exhibited high saturation magnetization, low dielectric constant low dielectric loss and narrow FMR linewidth [35]. Ning et al. demonstrated that the addition of Bi_2O_3

could greatly reduce sintering temperature, and enhance the grain growth at the same time [16]. Wang et al. revealed that the dielectric constant of the samples showed little variation with Mn concentrations and the addition of Mn with proper quantity could improve magnetic properties of YIG ferrites significantly [36].

Based on previous literatures, some elements such as Mn, Zr and Ca has been proved to be excellent substituting agents, which could enhance the saturation magnetization and decrease FMR linewidth. Besides, Bi_2O_3 is also widely used and considered to be an effective fluxing. Hence, Mn, Zr and Ca elements were also involved in our work to improve the properties of YIG products. Concerning dopant concentrations, they were based on the principle of preserving the intact garnet YIG phase and coordinating the valence to obtain YIG ferrites with better properties, and the dopant concentrations in literatures were also important criteria for reference. However, the existing studies pay little attention to Ce-substituted YIG ferrites, and the effects of Ce contents on kinds of properties of YIG ferrites have not been reported in detail. Therefore, in this study, except for Ca-Mn-Zr dopants, Ce element was also introduced into the YIG ferrites ceramics, whose concentration increased from $x = 0$ up to $x = 0.5$, providing a considerable range of

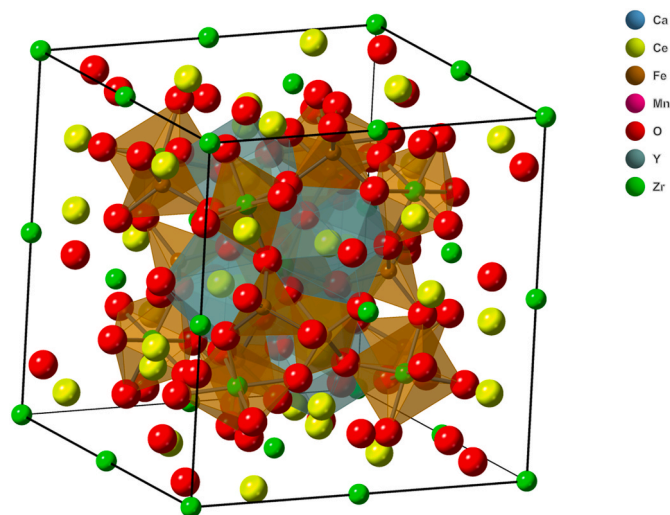


Fig. 2. Schematic illustration of a garnet unit cell.

relevant data. The effects of Ce contents on crystal phase, microstructure and magnetic properties of prepared YIG ferrites were investigated, and the influences of sintering temperature were also discussed.

2. Experimental

In this work, YIG ferrite ceramics with a composition of $\text{Ca}_{0.3}\text{Ce}_x\text{Y}_{2.7-x}\text{Mn}_{0.05}\text{Zr}_{0.45}\text{Fe}_{4.5}\text{O}_{12}$ ($x = 0, 0.05, 0.1, 0.2, 0.3, 0.4, 0.5$) were synthesized by solid-state reaction method. The raw materials include Fe_2O_3 , Y_2O_3 , CaCO_3 , MnO , Bi_2O_3 , CeO_2 , ZrO_2 (99 % AR-grade), and they were weighed according to stoichiometric ratio and mixed with deionized

water. The mixtures were then ball-milled for 4 h using a planetary ball mill. After drying for 24 h at 70 °C, the mixtures were pre-sintered for 2 h. Subsequently, a certain amount of Bi_2O_3 (1.0 wt %) was weighed and used as a fluxing agent for subsequent sintering. Then the pre-sintered products and Bi_2O_3 were further ball-milled for 4 h to make them more homogeneous, after that, they were completely dried and pelletized using 15 wt % polyvinyl alcohol (PVA) as a binder. Next, the granulated products were pressed and molded. Finally, the pressed samples were sintered at 1280 °C for 3.5 h in air. Meanwhile, another batch of samples were sintered at 1230 °C for 3.5 h in air in order to compare.

The Crystalline structures of all samples were scanned by an X-ray diffractometer (XRD, D/max 2400, Rigaku, Japan) with a Cu K radiation source and the scanning range of was $2\theta = 10\text{--}80^\circ$. Scanning electron microscope (SEM, JSM 6490, JEOL, Japan) was used to study the structure of the fracture cross sections of the samples. The density of the prepared YIG ferrites was measured by the classical Archimedes method. The magnetic hysteresis (M - H) loops of the samples were measured using a vibrating sample magnetometer (VSM) with an applied magnetic field ranging from -3200 Oe to 3200 Oe. Ferromagnetic resonance (FMR) linewidths of the samples were measured via the perturbation method, and the samples were crushed and ground to obtain spherical specimens with a diameter of 1 mm.

3. Results and discussion

Fig. 1 shows XRD diffraction patterns of the samples with different Ce concentrations sintered at different temperatures in the range of $10\text{--}80^\circ$, and they are compared with those of the standard card of YIG phase (PDF#43-0507). It can be seen that Fig. 1 (a) and 1 (b) have almost identical patterns, indicating that the samples sintered at different temperatures form the same phase. Clear diffraction peaks

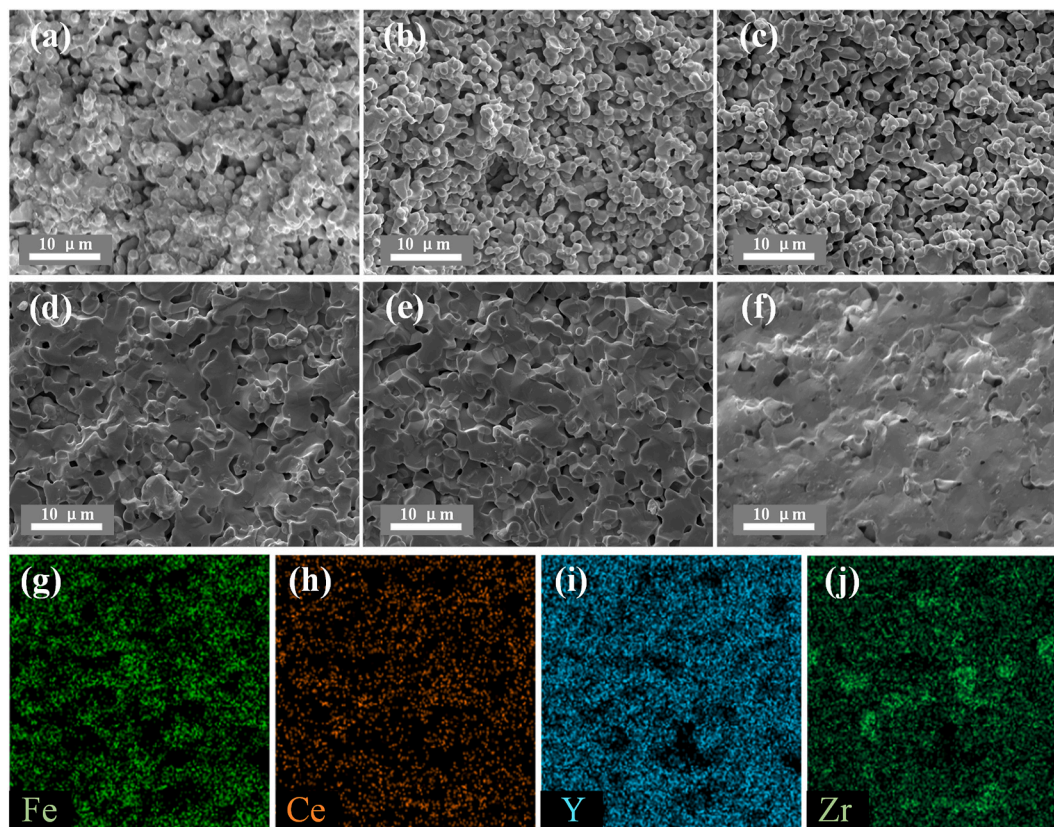


Fig. 3. SEM images of the prepared $\text{Ca}_{0.3}\text{Ce}_x\text{Y}_{2.7-x}\text{Mn}_{0.05}\text{Zr}_{0.45}\text{Fe}_{4.5}\text{O}_{12}$ samples sintered at 1280 °C with different doping concentrations: (a) $x = 0$, (b) $x = 0.05$, (c) $x = 0.1$, (d) $x = 0.3$, (e) $x = 0.4$, (f) $x = 0.5$; and corresponding mapping results of (g)–(j).

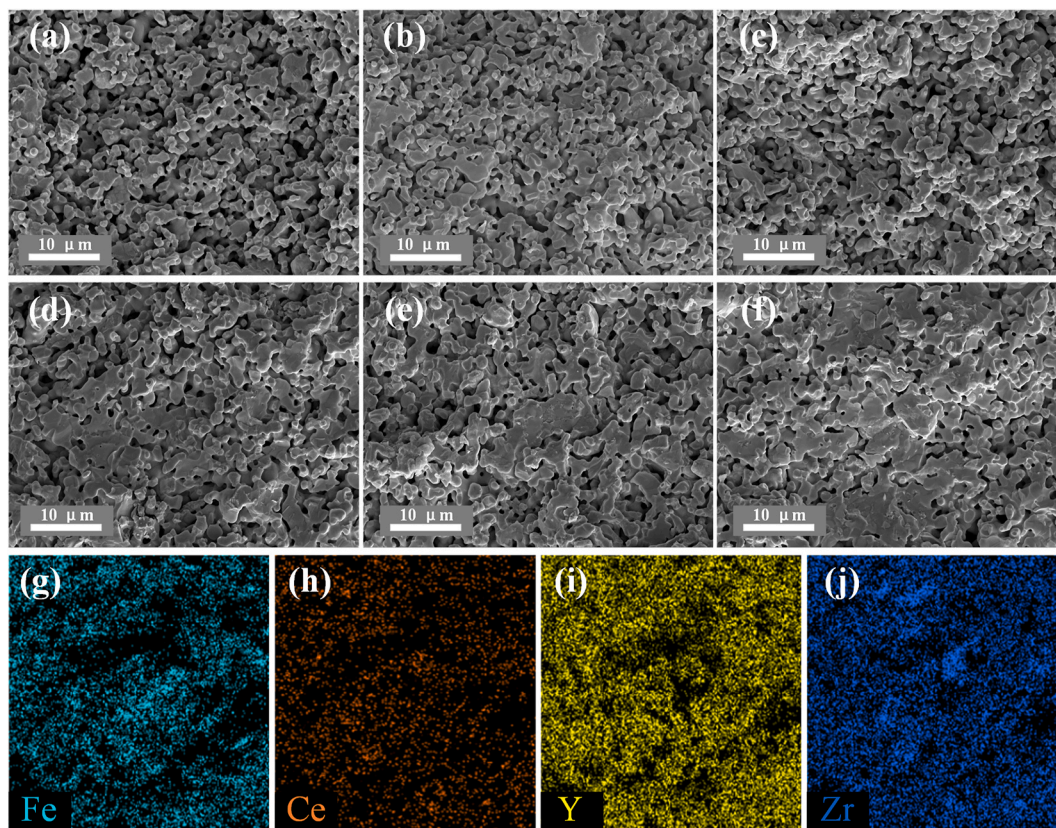


Fig. 4. SEM images of the prepared $\text{Ca}_{0.3}\text{Ce}_x\text{Y}_{2.7-x}\text{Mn}_{0.05}\text{Zr}_{0.45}\text{Fe}_{4.5}\text{O}_{12}$ samples sintered at $1230\text{ }^\circ\text{C}$ with different doping concentrations: (a) $x = 0$, (b) $x = 0.05$, (c) $x = 0.1$, (d) $x = 0.3$, (e) $x = 0.4$, (f) $x = 0.5$; and corresponding mapping results of (g)–(j).

locating at 17.51° , 28.78° , 32.27° , 35.41° , 39.75° , 45.01° , 50.92° , 53.22° , and 55.34° are detected in all the samples, matching well with the patterns of PDF #43–0507, which can be indexed to the (211), (400), (420), (422), (521), (532), (444), (640), and (642) planes of garnet phase. Besides, a diffraction peak exists near 29° , which is analyzed to be a possible phase of ZrO_2 . Rietveld refinement of the XRD patterns of samples sintered at $1230\text{ }^\circ\text{C}$ and $1280\text{ }^\circ\text{C}$ are presented in Fig. 1 (c) and (d) Rietveld refinement of the XRD patterns. It can be seen that not only the main peaks are consistent with YIG but also the peak near 29° is in accordance with ZrO_2 . The wt. fraction of ZrO_2 , presented by refinement, is very small, only about 3.7 %. For the sample sintered at $1230\text{ }^\circ\text{C}$, the adjustment parameters after refining by using Rietveld are as follow: $w_r = 6.848$, $\chi^2 = 1.07$. For the sample sintered at $1280\text{ }^\circ\text{C}$, the adjustment parameters after refining by using Rietveld are as follow: $w_r = 6.148$, $\chi^2 = 1.10$. These indicate an adequate quality of Rietveld's refinement and that the results are plausible. The analysis was released combining the data from measured diffractograms and the standard record from Crystallography Open Database (COD). Hence, it can be concluded that the prepared ferrites whether sintered at $1230\text{ }^\circ\text{C}$ or $1280\text{ }^\circ\text{C}$ could all form a YIG phase.

Fig. 2 shows Schematic illustration of a garnet YIG unit cell. The unit cell of YIG ferrite has 64 metal cations and 96 O ions, making a total of 160 ions. In this case, the Zr and Ce ions replace the Y^{3+} ion at the c-site of the dodecahedron, and the Mn and Zr ions replace the Fe^{3+} ion at the a-site of the octahedron. With the addition of dopants, Fe^{2+} ions that may be located on the tetrahedral or octahedral sites are produced. The addition of these dopant ions resulted in a significant improvement in the densification and magnetic properties of the YIG samples. It should be noted the XRD patterns have negligible changes with the increase of Ce concentrations, indicating that the introduction of Ce would not deteriorate the crystal structure of YIG ferrites. On the other hand, the introduction of Ce would significantly affect morphologies of YIG

products, which will be discussed below.

Fig. 3 shows SEM morphologies of the prepared YIG ferrites samples with different Ce doping concentrations at a sintering temperature of $1280\text{ }^\circ\text{C}$. Regarding the sample without Ce doping, as shown in Fig. 3 (a), the grain sizes are relatively small, resulting in a poor densification. With the introduction of Ce dopants ($x = 0.05$ and 0.1), as shown in Fig. 3(b) and (c), ferrites grains began to become larger, resulting from the existence of Ce ions that could promote the grain growth. Nevertheless, due to the insufficient doping contents, there are still a large number of small particles and the densification degree is still poor. Further increasing the Ce concentration ($x = 0.3$ and 0.4), as shown in Fig. 3 (d) and 3 (e), larger grains could be remarkably observed, and the densification is also enhanced at the same time. However, with the doping amount of $x = 0.5$, although most of the pores disappear, grain conglutination emerges and the grain boundaries become indistinct. Fig. 3(g–j) exhibit the mapping results concerning Fe, Ce, Y, and Zr elements, in which those elements are evenly distributed.

As for the samples sintered at $1230\text{ }^\circ\text{C}$, the morphologies are displayed in Fig. 4(a)–(f). The same phenomena compared with that of Fig. 3 is that the YIG ferrites grains become larger with the assistance of Ce dopant. The difference is that the densification is hardly to be improved with the increase of Ce dopant for the samples sintered at $1230\text{ }^\circ\text{C}$, where plenty of pores could still be observed in all the samples. It is noted that a homogeneous element distribution could also be obtained even at a relatively low sintering temperature (Fig. 4(g)–(j)). Therefore, we can conclude that (i) an appropriate sintering temperature is a key issue to obtain satisfying microstructures, and a higher temperature can usually promote the grain growth and lead to larger ferrites grains; (ii) the content of Ce dopant also plays an important role in morphology of YIG ferrites. This could be attributed to the substitution of Ce for Y in the 24c dodecahedral position in YIG and the partial oxidation of Ce^{3+} to Ce^{4+} in the grain boundary region and the

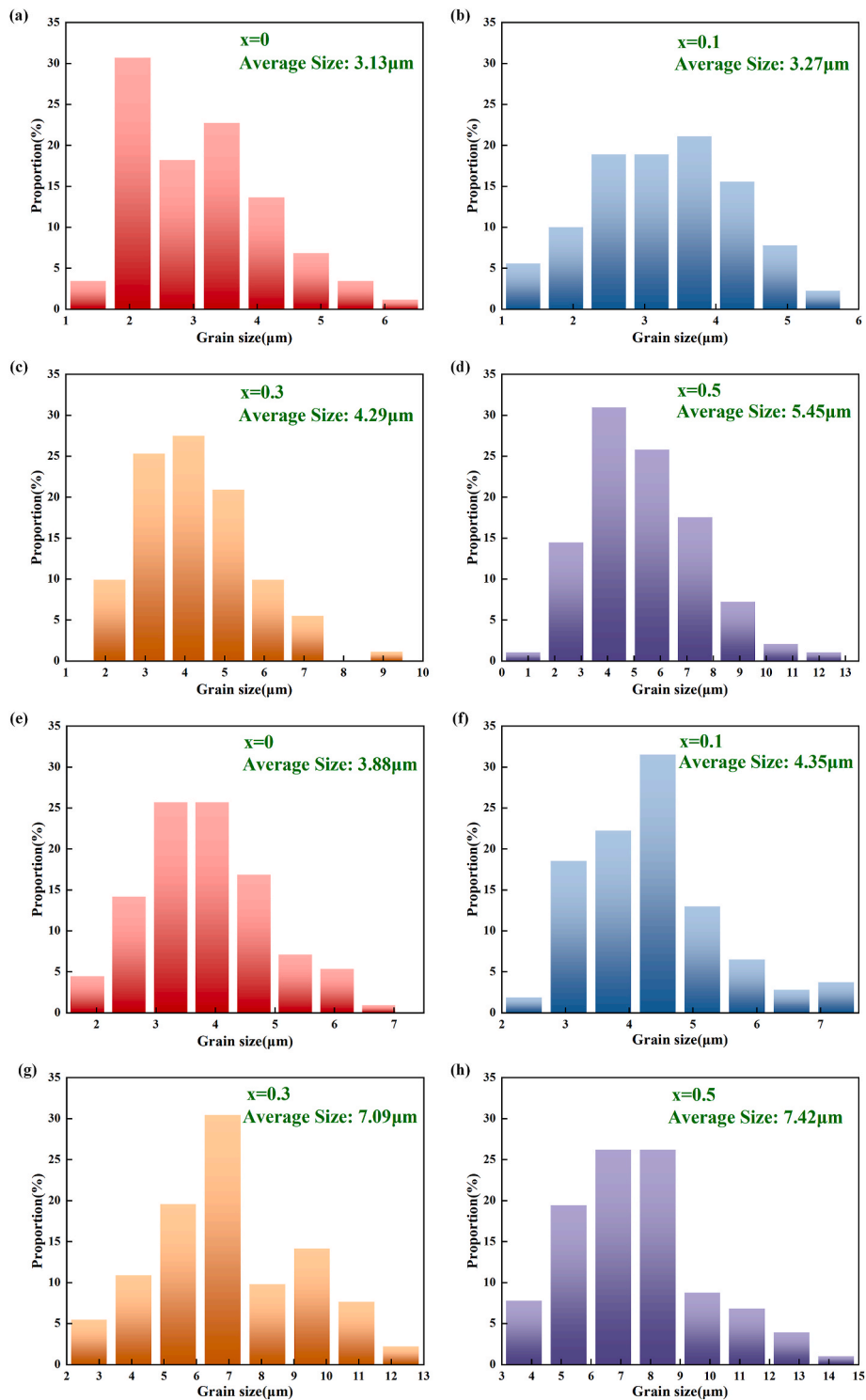


Fig. 5. Histograms for grain size distribution of the $\text{Ca}_{0.3}\text{Ce}_x\text{Y}_{2.7-x}\text{Mn}_{0.05}\text{Zr}_{0.45}\text{Fe}_{4.5}\text{O}_{12}$ products with different Ce doping concentrations: (a)–(d) sintered at 1280 °C, (e)–(h) sintered at 1230 °C.

appearance of cationic cavities to balance the potential difference, which increase the rate of grain boundary movement and contribute to grain growth during sintering. However, excessive addition would bring adverse effects. The excessive substitution of Ce for Y requires more energy to form covalent bonds, which could obstruct crystallinity. Therefore, appropriate amount of Ce dopant could improve crystallinity and make the crystal grains large.

Fig. 5 demonstrates the histograms of grain size of samples sintered

at 1230 °C and 1280 °C. In Fig. 5 (a), the average grain size is 3.88 μm when the doping amount is $x = 0$, and more than 50 % of the grains have a grain diameter less than 4 μm, in good coincidence with the SEM image in Fig. 3 (a). The average grain size increases to 4.35 μm when the doping amount is $x = 0.1$ (Fig. 5 (b)), which shows a small increase of grain size and a significant decrease in the proportion of small grains. However, the proportion of grains with a large size is still low that only 6.5 % of the grains have diameters larger than 6.2 μm.

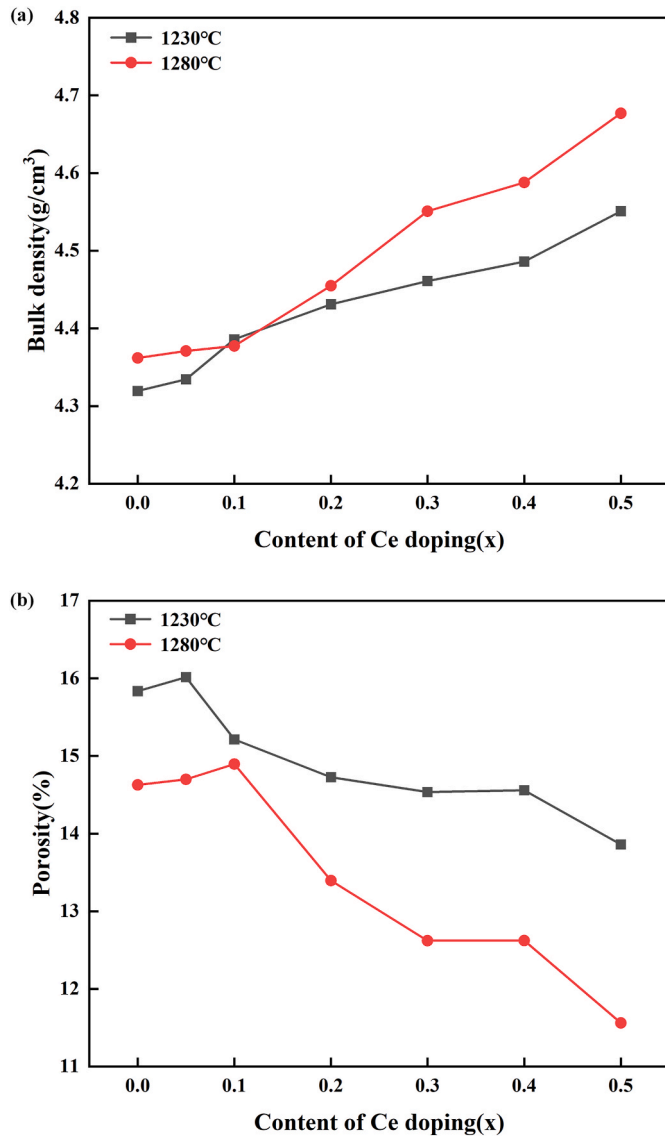


Fig. 6. (a) Bulk density and (b) porosity of samples with different Ce doping concentrations sintered at different temperatures.

Further increasing the Ce doping amount to $x = 0.3$ (Fig. 5 (c)), the average grain size increases significantly to $7.09 \mu\text{m}$, and more than 80 % of grains larger than $4 \mu\text{m}$ are obtained. Although the average grain size could reach up to $7.42 \mu\text{m}$ when $x = 0.5$ (Fig. 5 (d)), the conglutination effect is severe and would bring about adverse effects on YIG properties. Regarding the samples sintered at 1230°C (Fig. 5(e-h)), the average grain size shows a similar trend. Specifically, the average grain size increases from $3.13 \mu\text{m}$ to $5.45 \mu\text{m}$ with the Ce doping concentration increased from $x = 0$ to $x = 0.5$. In the condition of $x = 0.3$, the average grain size is $4.29 \mu\text{m}$, and more than 90 % of the grains with a diameter larger than $3 \mu\text{m}$. In contrast, the average grain size is $7.09 \mu\text{m}$ with the same amount of Ce dopant for the samples sintered at 1280°C . Clearly, the average grain size could be remarkably increased with a higher sintering temperature, and a higher proportion of large-size grains could also be obtained, in good accordance with the SEM images.

Fig. 6 shows the variation of bulk density and porosity with different Ce doping concentrations for samples sintered at different temperatures. Porosity of the prepared YIG ferrites can be determined by equation (1) [37]:

$$P = \frac{\rho_x - \rho_b}{\rho_x} \times 100\% \quad (1)$$

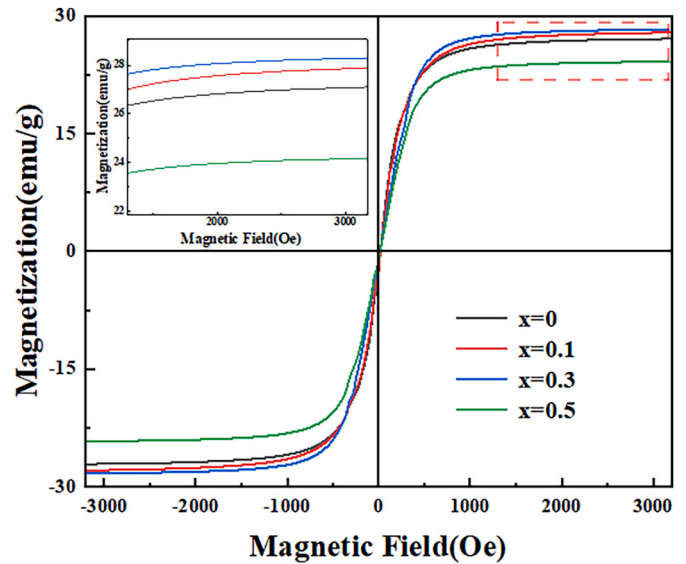


Fig. 7. Room temperature magnetization curves of $\text{Ca}_{0.3}\text{Ce}_x\text{Y}_{2.7-x}\text{Mn}_{0.05}\text{Zr}_{0.45}\text{Fe}_{4.5}\text{O}_{12}$ ferrites with different Ce doping concentrations.

where ρ_x and ρ_b represents the theoretical density and actual density, respectively. As shown in Fig. 6 (a), bulk densities of the samples increase all the time with the increase of Ce content. The bulk density of the sample sintered at 1280°C has increased from 4.36 g/cm^3 to 4.68 g/cm^3 when the Ce concentration increased from $x = 0$ to $x = 0.5$. Meanwhile, the corresponding porosity reduced from 14.6 % to 11.5 %, matching well with the SEM results. The increase of bulk density and decrease of porosity could be attributed to the existence of Ce dopant, which would promote the grain growth. Although the bulk density and porosity of the samples sintered at 1230°C show a similar trend, their bulk densities are lower and porosities are higher compared with those of the samples sintered at 1280°C , where the maximum bulk density is 4.55 g/cm^3 and the minimum porosity is 13.9 %.

On the whole, the introduction of Ce dopant can significantly increase the bulk density and reduce the porosity, in other words, the densification degree of YIG ferrites would be enhanced with the assistance of Ce dopant. Additionally, it can be concluded that a higher sintering temperature can usually lead to the ferrite ceramics with a more satisfying densification.

Fig. 7 shows the room temperature hysteresis loop ($M-H$ curves) for samples with different Ce doping concentrations at a sintering temperature of 1280°C . The coercivity can be read from the hysteresis loop ($M-H$ curves) diagram. When the magnetization of a magnetic body is 0, the coercivity can be read from the intersection of the hysteresis loop with the horizontal axis. The theoretical value of coercivity H_c is mainly determined by the displacement of the magnetic domain wall and the rotation of the magnetic moment, and its magnitude can be expressed as Equation (2):

$$H_c = 3 \left(\frac{KT_c K_1}{a M_s} \right) \left(\frac{1}{D} \right) \quad (2)$$

Where K is the anisotropy constant, T_c is the Curie temperature, K_1 is the first magnetic crystal anisotropy constant, a is the lattice constant, M_s is the saturation magnetization, and D is the grain size. From Fig. 7, it can be read that the coercivity decreases gradually with the increase in Ce concentration. When the doping concentration $x = 0$, the coercivity is 19.6 Oe and then, the coercivity decreases to 14.7 Oe at $x = 0.5$. Ce ion doping alters the microscopic morphology and particle size of YIG so that the YIG material's coercivity reduced.

The theoretical value of saturation magnetization (M_s) can be calculated by Equation (3)

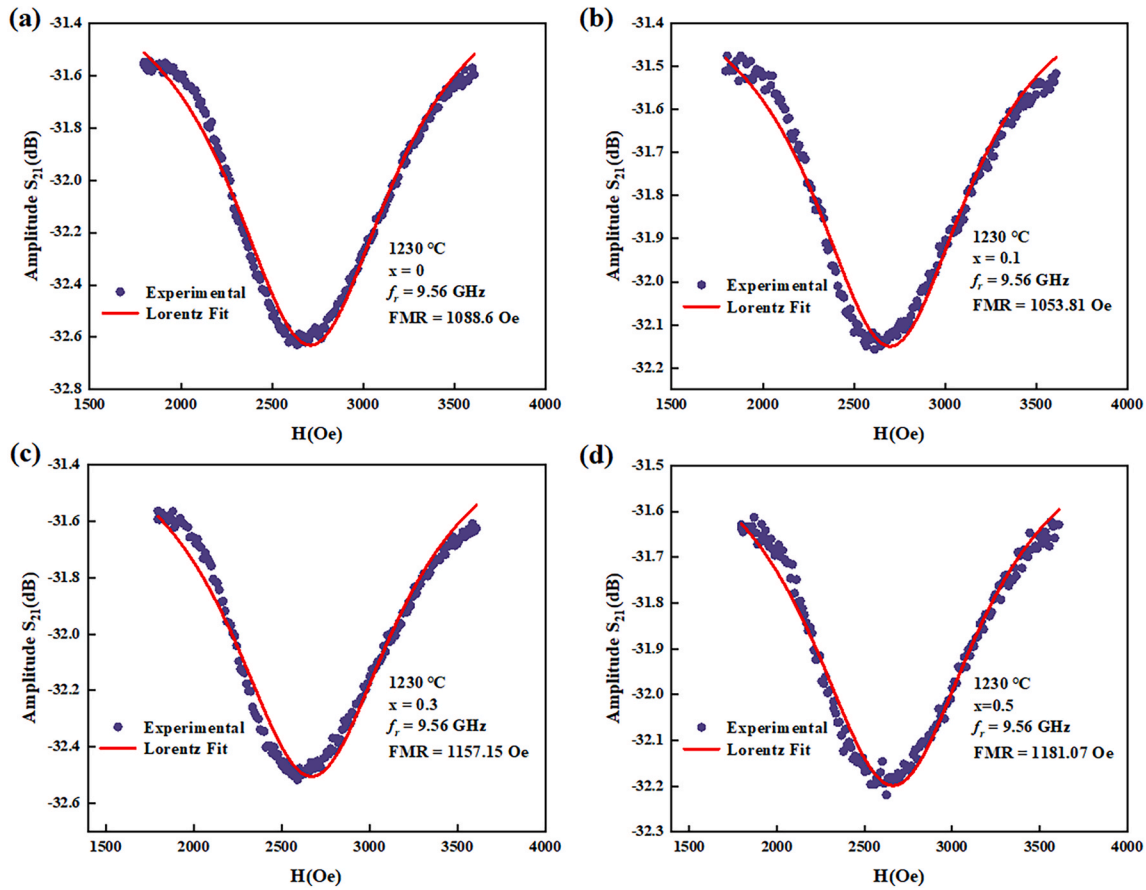


Fig. 8. FMR linewidth of the samples with different doping concentrations sintered at 1230 °C.

$$M_S = \frac{8n\mu_B}{10^3 a^3 \rho} \quad (3)$$

where n is the theoretical number of magnetic moments per formula unit, μ_B is the magnitude of Bohr magneton, a is the lattice parameter, ρ is the density. The saturation magnetization also can be read from the hysteresis loop (M - H curves) diagram. When the applied magnetizing force increases while the magnetizing strength of the material remains constant, the magnetization is called saturation magnetization. Various factors influencing the saturation magnetization of doped ferrites, such as crystallite size, particle size and so on. The magnetization value increases rapidly in the range of 0–1000 Oe, after exceeding 1000 Oe, the magnetization value gradually stabilizes. Besides, the introduction of Ce dopant has a significant effect on the magnetization of YIG ferrite ceramics. Specifically, the saturation magnetization of the sample sintered at 1280 °C without Ce dopant is 27.1 emu/g, then the saturation magnetization increases to 27.5 emu/g when the Ce content is $x = 0.1$. Further increasing the Ce content to $x = 0.3$, the saturation magnetization reaches a maximum value of 28.3 emu/g. However, the saturation magnetization decreases when excessive Ce dopant involved, in which only a value of 24.2 emu/g could be obtained when the dopant content is $x = 0.5$. The reason for the variation of saturation magnetization intensity can be explained by Néel's theory [38]. It is well known that in garnet crystal structure, magnetic moments of the three Fe ions at d -sites are antiparallel to magnetic moments of the two Fe ions at a -sites and the three Y ions at c -sites. The magnetic moment of ions has a temperature dependence. Therefore, those are described as a function of temperature expressed by Equation (4):

$$n_B = 3m_c(T)\mu_B + \{2m_a(T)\mu_B - 3m_d(T)\mu_B\} \quad (4)$$

where n_B is the magnetic moment per formula unit, μ_B is the Bohr

magneton, and m_c , m_a and m_d are the spin number of each ion in the c site, a site (Fe^{3+} site) and d site (Fe^{3+} site), respectively [39]. The magnetic properties of ferrites are mainly affected by ionic saturation magnetic moment and ionic occupation of sites in the crystal. Since Y ions are diamagnetic with a magnetic moment of $0 \mu_B$ ($m_c(T) = 0$ in Eq. (4)). By considering the relation $m_d(T) \cong m_a(T) \equiv m(T)$ for the temperature dependence of the spin magnetic moment, the net magnetic moment can be expressed by Equation (5):

$$n_B(T)_{YIG} = -1 \times m(T)\mu_B \quad (5)$$

Since Ce ions are paramagnetic and its magnetic moment is $1 \mu_B$, in the condition of an appropriate amount of Ce dopant involved, they will enter the dodecahedral position c -sites and replace a portion of Y ions. When Mn and Zr are substituted for d site Fe, $n_B(T)$ will be expressed as follows:

$$|n_B(T)_{Ce:YIG}| = |0.5 \times m_c(T)\mu_B - 0.5 \times m(T)\mu_B| \quad (6)$$

Based on equation (6), it can be concluded that the substitution of nonmagnetic Y ions by magnetic Ce ions will lead to the increase of m_c , which will then cause the decrease of total magnetic moment. Therefore, theoretically, the saturation magnetization will decrease with the increase of Ce dopant concentration. However, when $x = 0, 0.1, 0.2$ and 0.3 , the saturation magnetization did not vary much, just increase slightly from 27.1 emu/g to 28.3 emu/g. This can be attributed to the distortion of the structure caused by the Ce^{3+} , which allows a modification of the magnetization through the modification of superexchange interactions between octahedral and tetrahedral sites; in particular, the lengths and angle of the Fe-O-Fe bonds change, modifying the net magnetic moment of the material. As the doping of Ce continued to increase to $x = 0.5$, more Ce are introduced in c site, which increase the total magnetic moments of cations in dodecahedral sites. Thus, the

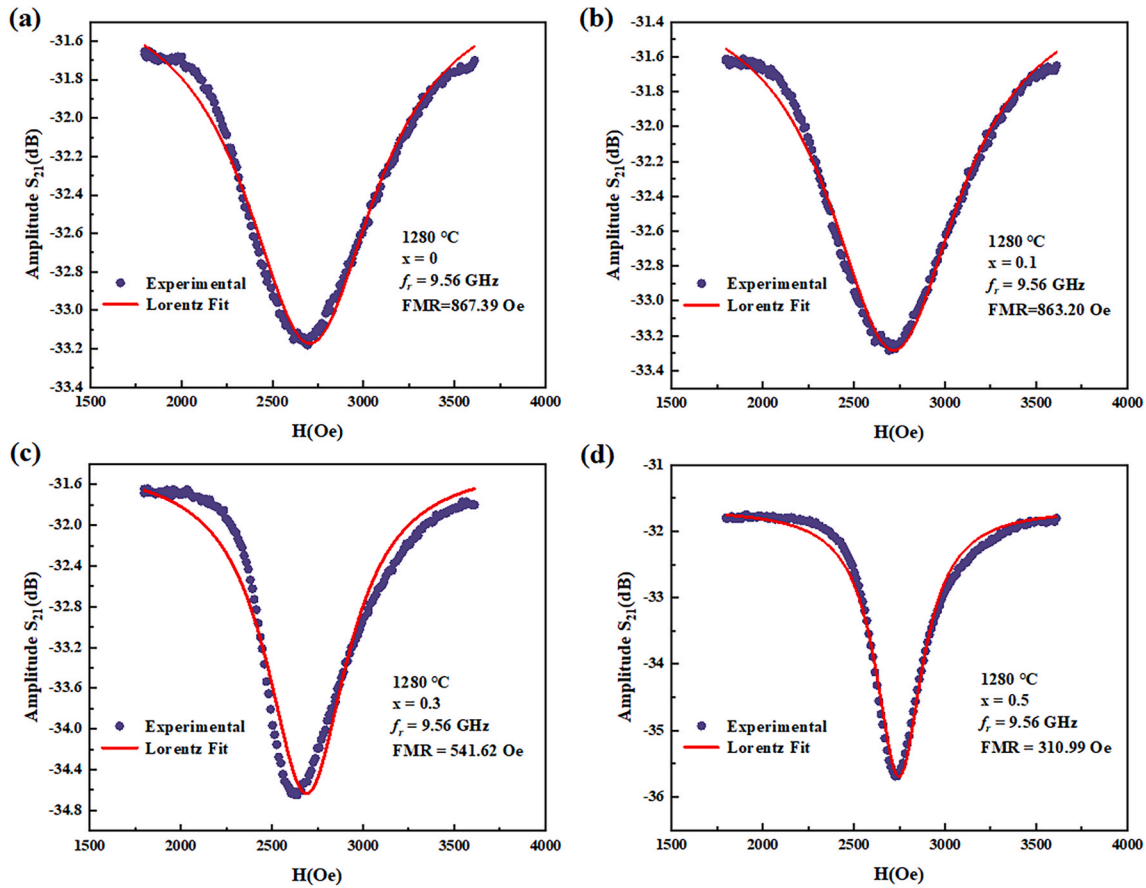


Fig. 9. FMR linewidth of the samples with different doping concentrations sintered at 1280 °C.

saturation magnetization decreased distinctly to 24.2 emu/g. Except for the ion substitution that can affect the magnetization, the densification degree will also play a vital role. For example, regarding the samples sintered at 1230 °C, a maximum value of only 18.0 emu/g can be obtained, which is much lower than that of the YIG ferrites sintered at 1280 °C. It can be explained that magnetization is also influenced by bulk density, porosity and grain size, the density of the products sintered at 1280 °C is higher and porosity is smaller, hence the samples possess a better densification and exhibit higher magnetization values. Therefore, sintering temperature and Ce concentration are both vital factors that will significantly influence the magnetization value, and an appropriate amount of Ce dopant is essential to obtain YIG ferrites with better magnetization performances.

Fig. 8 shows the ferromagnetic resonance (FMR) linewidths (ΔH) of the samples sintered at 1230 °C, and the values of ΔH were obtained based on Lorentzian fitting. First, all of the samples exhibit a relatively high ΔH value (more than 1000 Oe), which is unsatisfying for YIG ferrites. Second, it can be seen that the introduction of Ce dopant has no obvious influences on ΔH value. It could be attributed to the fact that the samples sintered at relatively low temperatures are immature that densification is poor and grain size is small, whose influences outweigh the effect of Ce dopant. In contrast, the samples sintered at 1280 °C show better performances on FMR linewidth, as shown in Fig. 9. Obviously, ΔH values of the samples sintered at 1280 °C are all lower than that of the samples sintered at 1230 °C, in the condition of same Ce dopant content. From this perspective, sintering YIG ferrite ceramics at a relatively high temperature is necessary to obtain good YIG products. Another significant difference is that the ΔH values of the samples sintered at 1280 °C are highly dependent on Ce dopant concentrations. Specifically, the ΔH value of the prepared YIG sample is 867.3 Oe when no Ce dopant involved ($x = 0$). Then, the ΔH value sharply decreases to

541.6 Oe when the amount of Ce dopant is $x = 0.3$. Further increasing Ce concentration, the ΔH value can reach to 310 Oe when the amount of Ce dopant is $x = 0.5$.

For high-frequency ferrite materials, magnetic loss is usually characterized by FMR linewidth ΔH . It depends on the resonance frequency f_r as $\Delta H = (2/\gamma_0)\alpha f_r$, where f_r is the resonance frequency, α is damping and γ_0 is the reduced gyromagnetic ratio [40]. In order to more succinctly articulate the reasons for the narrowing of the FMR linewidth, the FMR linewidth ΔH could be expressed by Equation (7):

$$\Delta H = \Delta H_i + \Delta H_a + \Delta H_p + \Delta H_s + \Delta H_r + \Delta H_{inc} \quad (7)$$

where ΔH_i , ΔH_a , ΔH_p , ΔH_s , ΔH_r , and ΔH_{inc} represents the intrinsic, anisotropy, porosity, surface, fast relaxation, and solid-state reaction linewidth, respectively. Generally, the influence of ΔH_i can be ignored since the value of ΔH_i is much smaller compared with those of other factors. In addition, ΔH_s and ΔH_r can be disregarded due to the sample being ground into a sphere and polished at the surface before testing [41]. Besides, ΔH_{inc} can be mostly eliminated when the solid-phase reaction is sufficiently completed. Therefore, the main factors that would affect FMR linewidth of YIG ferrites are ΔH_a and ΔH_p . As for ΔH_a , it can be calculated by Equations (8) and (9):

$$H_a = \frac{K_1}{\mu_0 M_s} \quad (8)$$

$$\Delta H_a \approx 2.07 \frac{H_a^2}{M_s} G(\omega, \omega_i) \quad (9)$$

where K_1 represents the magnetic anisotropy constant, and $G(\omega, \omega_i)$ is a factor which depends on the frequency and M_s , which is nearly equal to 1 at high frequencies. In the condition of Ce dopant involved, larger Ce

ions would enter into the dodecahedral sites and replace Y ions, which could decrease the value of K_1 [42]. On the other hand, based on the previous results, the existence of Ce dopant would decrease the M_s value. Consequently, the value of ΔH_a may slightly increase with the increase of Ce doping content. As for ΔH_p , it is mainly resulted from the porosity of ferrites, and the value of ΔH_p and porosity degree are positively correlated [43]. Therefore, reducing porosity degree is essential in order to obtain a lower ΔH_p value. The SEM and density results discussed before all indicate that the introduction of Ce dopant can significantly reduce the porosity degree, which will correspondingly decrease the ΔH_p value. ΔH_p declined more than ΔH_a with the increase of Ce doping content, which indicated that ΔH will decrease accordingly. In total, an appropriate amount of Ce dopant can reduce magnetic anisotropy constant K_1 , promote grain growth that can improve the densification and reduce the porosity degree, so as to reduce the values of ΔH of the prepared YIG ferrites.

4. Conclusion

In this study, $\text{Ca}_{0.3}\text{Ce}_x\text{Y}_{2.7-x}\text{Mn}_{0.05}\text{Zr}_{0.45}\text{Fe}_{4.5}\text{O}_{12}$ ferrite ceramics were synthesized via the solid-state sintering method at different temperatures of 1230 °C and 1280 °C. The results indicated that the introduction of Ca, Ce, Mn, and Zr elements did not deteriorate the YIG crystal phase, while the microstructure and magnetic properties were highly depended on the content of Ce dopant. Therefore, Ce doping can significantly promote the grain growth and enhance the density of the prepared YIG ferrite. Besides, in terms of magnetic properties, Ce doping increases the saturation magnetization of the sample sintered at 1280 °C (from 27.1 to 28.3 emu/g), and significantly decreases the FMR linewidth from 867.3 Oe to 310 Oe. By considering the low sintering temperature of 1280 °C, the YIG ferrite synthesized in this work achieved relatively good magnetic properties. The inferior performance in most magnetic properties of the sample sintered at 1230 °C can prove that the sintering temperature is a key factor, but more importantly, the introduction of Ce dopant could promote grain growth and then improved magnetic properties. The decrease of more 50 per cent of the linewidth (ΔH) indicated that the prepared $\text{Ca}_{0.3}\text{Ce}_x\text{Y}_{2.7-x}\text{Mn}_{0.05}\text{Zr}_{0.45}\text{Fe}_{4.5}\text{O}_{12}$ ferrite ceramics could be tailored to obtain good properties and be hopeful to be applied in microwave components.

CRedit authorship contribution statement

Xiaoyi Wang: Writing – review & editing, Supervision, Resources, Project administration, Methodology, Investigation. **Kun Xu:** Writing – original draft, Investigation. **Ning Ma:** Data curation. **Xiujuan Feng:** Methodology. **Gang Zhou:** Supervision. **Gang Chen:** Data curation. **Lei Zhao:** Funding acquisition, Resources.

Declaration of competing interest

The authors declare that they have no known competing financial interests or personal relationships that could have appeared to influence the work reported in this paper.

Acknowledgements

This work was supported by National Key Research and Development Program of China (No. 2021YFC2902701, 2021YFC2902100), Shandong Provincial Major Science and Technology Innovation Project (No. 2021CXGC011206), and Key Projects of National Natural Science Foundation of China (52130402).

References

- [1] Z.M. Temesvári, D. Maros, P. Kádár, Review of Mobile communication and the 5G in manufacturing, *Procedia Manuf.* 32 (2019) 600–612.
- [2] Q. Chen, P. Lin, X. Du, H. Inoue, K. Kizaki, T. Lin, P. He, A new strategy to fabricate YIG ferrite joint with novel magnetic $\text{Bi}_2\text{O}_3\text{-CoO-Fe}_2\text{O}_3\text{-B}_2\text{O}_3$ glass, *Mater. Des.* (2022) 215.
- [3] Y. Hu, X. Liu, S. Feng, L. Zen, Ferromagnetic resonance linewidth mechanism of Sr–Sn substituting YIG ferrite, *J. Mater. Sci. Mater. Electron.* 33 (2022) 14663–14671.
- [4] Z. Li, G. Liu, H. Yang, F. Liu, S. Yang, B. Dai, Y. Ren, F. Xu, C. Hu, Structure and properties of fiber-reinforced LiZn ferrite ceramics prepared via spark plasma sintering, *Ceram. Int.* 49 (2023) 34500–34509.
- [5] Y. Xiao, J. Li, T. Zhou, Y. Yang, K. Sun, Y. Liu, Mechanism of the impact of Ca–Ge co-substitution on the FMR linewidth in BiV–YIG ferrites, *Ceram. Int.* 50 (2024) 20144–20150.
- [6] Y. Lin, H. Yang, J. Zhu, F. Wang, Magnetic and dielectric properties of YIG/HDPE composites for high-frequency applications, *Int. J. Polym. Mater.* 59 (2010) 570–576.
- [7] W. Li, J. Li, X. Peng, J. Xu, Y. Yang, D. Jin, H. Jin, X. Wang, H. Ge, Improved permeability and decreased core loss of iron-based soft magnetic composites with YIG ferrite insulating layer, *J. Alloys Compd.* 937 (2023).
- [8] C. Guo, W. Zhang, R. Ji, Y. Zeng, Effects of In^{3+} -substitution on the structure and magnetic properties of multi-doped YIG ferrites with low saturation magnetizations, *J. Magn. Magn. Mater.* 323 (2011) 611–615.
- [9] F. Chen, Z. Zhang, X. Wang, J. Ouyang, Z. Feng, Z. Su, Y. Chen, V.G. Harris, Room temperature magnetoelectric effect of $\text{YFeO}_3\text{-Y}_3\text{Fe}_5\text{O}_{12}$ ferrite composites, *J. Alloys Compd.* 656 (2016) 465–469.
- [10] X. Han, J. Li, H. Wu, K. Sun, Y. Chen, L. Jia, H. Zhang, P. Zhang, C. Wu, High dielectric constant and magnetic properties of Bi–In Co-substituted YIG ferrites, *J. Magn. Magn. Mater.* 570 (2023) 170512.
- [11] W. Zhao, Y. Liu, Q. Yin, J. Li, S. Lu, P. Zhang, Z. Chen, Substitution modification mechanism of YIG ferrite with a high spin-wave linewidth via fast relaxation Dy^{3+} ion doping and sintering modulation, *J. Eur. Ceram. Soc.* 44 (2024) 116708.
- [12] R. Peña-García, Y. Guerra, F.R. de Souza, L.A.P. Gonçalves, E. Padrón-Hernández, The extended Bloch's law in yttrium iron garnet doped with Zn, Ni and Co, *Phys. E Low-dimens. Syst. Nanostruct.* 103 (2018) 354–360.
- [13] R. Peña-García, Y. Guerra, D.M. Oliveira, A. Franco, E. Padrón-Hernández, Local atomic disorder and temperature dependence of saturation magnetization in yttrium iron garnet, *Ceram. Int.* 46 (2020) 5871–5875.
- [14] L.R.F. Leal, R. Milani, D.M. Oliveira, Y. Guerra, E. Padrón-Hernández, A. Franco, B. C. Viana, F.E.P. Santos, R. Peña-García, Competitive effect of dopants on magnetic and structural properties in yttrium iron garnet co-doped with Er and Cr, *Ceram. Int.* 46 (2020) 18584–18591.
- [15] X. Wang, K. Xu, D. Cheng, X. Feng, Enhanced properties of $\text{Li}_{0.42}\text{Zn}_{0.27}\text{Ti}_{0.11}\text{Mn}_{0.1}\text{Fe}_{2.1}\text{O}_4$ ferrites co-fired with $\text{Bi}_2\text{O}_3\text{-B}_2\text{O}_3$ additive at low sintering temperatures, *Ceram. Int.* 49 (2023) 39465–39472.
- [16] N. Jia, Z. Huaiwu, J. Li, Y. Liao, L. Jin, C. Liu, V.G. Harris, Polycrystalline Bi substituted YIG ferrite processed via low temperature sintering, *J. Alloys Compd.* 695 (2017) 931–936.
- [17] V.G. Harris, *Modern Microwave Ferrites*, vol. 48, 2011, pp. 1075–1104.
- [18] X. Wang, K. Yin, T. Cao, Y. Liao, Z. Wang, Q. Kou, D.J.J.o.A. Cheng, Effects of $\text{Bi}_2\text{O}_3\text{-V}_2\text{O}_5$ mixture on microstructure and magnetic properties for $\text{Li}_{0.42}\text{Zn}_{0.27}\text{Ti}_{0.11}\text{Mn}_{0.1}\text{Fe}_{2.1}\text{O}_4$ ferrites sintered at low temperatures, *J. Alloys Compd.* 885 (2021) 160983.
- [19] J. Zhou, Y. Lin, H. Yang, Y. Ren, F. Xu, Structural, morphological and magnetic properties of low temperature sintered LiZnTiBi ferrites, *J. Alloys Compd.* 932 (2023) 167616.
- [20] M. Niaz Akhtar, M. Azhar Khan, M. Ahmad, G. Murtaza, R. Raza, S.F. Shaikat, M. H. Asif, N. Nasir, G. Abbas, M.S. Nazir, M.R. Raza, $\text{Y}_3\text{Fe}_5\text{O}_{12}$ nanoparticulate garnet ferrites: comprehensive study on the synthesis and characterization fabricated by various routes, *J. Magn. Magn. Mater.* 368 (2014) 393–400.
- [21] Y.-Y. Huang, J. Yang, T. Qiu, J.-Q. Wang, Y.-L. Jin, Effects of Zr-substitution on microstructure and properties of YCaVIG ferrites, *J. Magn. Magn. Mater.* 324 (2012) 934–938.
- [22] H. Wu, F. Huang, X. Lu, T. Xu, X. Lu, R. Ti, Y. Jin, J.P.s.s. Zhu, Grain Size and Fe^{2+} Concentration-Dependent Magnetic, Dielectric, and Magnetodielectric Properties of $\text{Y}_3\text{Fe}_5\text{O}_{12}$ Ceramics, vol. 213, 2016, pp. 146–153.
- [23] W.J. Sousa, Y. Guerra, R. Peña-García, E. Padrón-Hernández, Saturation magnetization as a function of temperature in Zn doped YIG nanoparticles, *Phys. E Low-dimens. Syst. Nanostruct.* 138 (2022).
- [24] A. Fernández, F.P. Araujo, Y. Guerra, S. Castro-Lopes, J. Matilla-Arias, I.S. de Lima, E.C. Silva-Filho, J.A. Osajima, F. Guerrero, R. Peña-García, Synthesis of coral-like structures of Pr–Yb co-doped YIG: structural, optical, magnetic and antimicrobial properties, *J. Rare Earths* 42 (2024) 543–554.
- [25] C. Alves, J. Matilla-Arias, F. Guerrero, S. Castro-Lopes, Y. Guerra, B.C. Viana, E. Padrón-Hernández, J.M. Soares, R.B. da Silva, M.G. Ghislandi, R. Peña-García, Influence of Fe^{3+} by La^{3+} cations substitution on the crystallography and magnetic properties of yttrium iron garnet compound, *Ceram. Int.* 49 (2023) 27567–27576.
- [26] L. Leal, J. Matilla-Arias, Y. Guerra, C.S. Oliveira, S. Castro-Lopes, B.C. Viana, G. Abreu, P. Marino-Castellanos, F. Santos, R. Peña-García, Oxidation states and occupation sites of Fe and Cu ions in the $\text{Y}_3\text{Fe}_{5-x}\text{Cu}_x\text{O}_{12}$ ($0.00 \leq x \leq 0.05$) compound synthesized via sol gel method, *J. Alloys Compd.* (2022) 915.
- [27] Y. Guerra, L. Leal, M. Cabrera-Baez, E. Padrón-Hernández, S. Castro-Lopes, B. C. Viana, G. Abreu, J. Caland, P. Matos-Rodrigues, F. Santos, J. Matilla-Arias, R. Peña-García, Cation distribution, $\text{Fe}^{2+}/\text{Fe}^{3+}$ valence states and oxygen vacancies detection in the $\text{Y}_{2.98}\text{Er}_{0.02}\text{Fe}_{5-y}\text{Cr}_y\text{O}_{12}$ compound, *J. Alloys Compd.* (2023) 960.
- [28] M.N. Akhtar, M. Yousaf, S. Khan, M. Nazir, M. Ahmad, M.A. Khan, Structural and electromagnetic evaluations of YIG rare Earth doped (Gd, Pr, Ho, Yb) nanoferrites for high frequency applications, *Ceram. Int.* 43 (2017) 17032–17040.

- [29] J. Li, Y. Sun, F. Gao, H. Su, X. Han, Z. Liang, H. Zhang, Q. Li, Enhanced FMR linewidth and magnetic properties of In^{3+} -doped YIG ferrite materials for microwave devices applications, *J. Magn. Magn Mater.* 538 (2021) 168318.
- [30] Y. Yang, Z. Yu, Q. Guo, K. Sun, R. Guo, X. Jiang, Y. Liu, H. Liu, G. Wu, Z. Lan, Thermomagnetization characteristics and ferromagnetic resonance linewidth broadening mechanism for Ca-Sn Co-substituted YIG ferrites, *Ceram. Int.* 44 (2018) 11718–11723.
- [31] R. Peña-García, A. Delgado, Y. Guerra, G. Duarte, L.A.P. Gonçalves, E. Padrón-Hernández, The synthesis of single-phase yttrium iron garnet doped zinc and some structural and magnetic properties, *Mater. Res. Express* 4 (2017).
- [32] J.P. Caland, C.P.C. Medrano, A. Caytuelo, E. Baggio-Saitovitch, F.J. Litterst, J. M. Soares, M. Cabrera-Baez, E. Padrón-Hernández, T. Marques, Y. Guerra, B. C. Viana, F.E.P. Santos, R. Peña-García, Preferential site occupancy of Ni ions and oxidation state of Fe ions in the YIG crystal structure obtained by sol-gel method, *J. Alloys Compd.* (2020) 849.
- [33] J. Li, Y. Sun, F. Gao, H. Su, X. Han, Z. Liang, H. Zhang, Q. Li, Enhanced FMR linewidth and magnetic properties of In^{3+} -doped YIG ferrite materials for microwave devices applications, *J. Magn. Magn Mater.* 538 (2021).
- [34] J. Wang, Y. Jin, J. Yang, Y. Huang, T. Qiu, Effect of ZrO_2 addition on the microstructure and electromagnetic properties of YIG, *J. Alloys Compd.* 509 (2011) 5853–5857.
- [35] F. Gao, J. Li, H. Su, Y. Sun, Y. Yang, G. Wang, X. Han, Q. Li, Low dielectric loss and narrow FMR linewidth of Ca-Ge co-substituted YInG ferrites for microwave device application, *J. Alloys Compd.* 885 (2021).
- [36] W. Jiaqian, Y. Jian, J. Yulong, Q. Tai, Effect of Manganese Addition on the Microstructure and Electromagnetic Properties of YIG, vol. 29, 2011, pp. 562–566.
- [37] Y. Xiao, J. Li, Y. Lei, K. Sun, Y. Chen, S. Wang, P.J.C.I. Zhang, Ca-Sn co-substituted BiIn-YIG Ferrite with Narrow FMR Linewidth for Microwave Device Application, vol. 50, 2024, pp. 1031–1037.
- [38] L. Wang, Z. Huang, H. Zhang, R.J.J.o.M. Yu, M. Materials, Phase and magnetic properties evolutions of $\text{Y}_{3-x}(\text{CaZr})_x\text{Fe}_{5-x}\text{O}_{12}$ by the sol-gel method 395 (2015) 73–80.
- [39] M. Imamura, H. Asada, R. Nishimura, D. Tashima, J. Kitagawa, Thermoelectric Characteristics of STE Generator Fabricated from LPE Bi-and Al-substituted YIG Films, vol. 58, 2021, pp. 1–11.
- [40] M. Imamura, H. Asada, R. Nishimura, Y. Kano, D. Tashima, J.J.J.o.M. Kitagawa, M. Materials, Characteristics of spin-thermoelectric Generators Enhanced by Incorporating Liquid Phase Epitaxial Bi-substituted YIG Films as a Ferrimagnetic Insulator, vol. 550, 2022 169081.
- [41] J. Li, Y. Yang, G. Wang, L. Guo, Y. Rao, G. Gan, H.J.C.I. Zhang, Enhanced Structure and Microwave Magnetic Properties of Mgzn Ferrite by Cd^{2+} Ion Substitution for LTCC Applications, vol. 46, 2020, pp. 6600–6604.
- [42] Q. Yin, Y. Liu, J. Wu, J. Li, J. Chen, S. Lu, K.J.C.I. Liu, Mechanistic Study of the Effect of Ca-Sn co-doping on the Microwave Dielectric Properties and Magnetic Properties of YIG, vol. 48, 2022, pp. 32827–32836.
- [43] W. Yang, L. Wang, Y. Ding, Q. Zhang, Narrowing of Ferromagnetic Resonance Linewidth in Calcium Substituted YIG Powders by $\text{Zr}^{4+}/\text{Sn}^{4+}$ Substitution, vol. 25, 2014, pp. 4517–4523.